Proceedings World Geothermal Congress 2020+1
Reykjavik, Iceland, April - October 2021

Assessing the Effects of Hydraulic Stimulation Strategies on Fault Reactivation and Induced Seismicity using Coupled Hydro-mechanical Models

Wassing B.B.T.[1], Gan Q.[2], Candela T.G.G.[1], Fokker P.A.[1]

TNO, Utrecht, the Netherlands, University of Aberdeen, Aberdeen, Scotland, UK

brecht.wassing@tno.nl

Keywords: Enhanced Geothermal Systems, hydraulic stimulation, fault reactivation, induced seismicity, poroelasticity.

ABSTRACT

Hydraulic stimulation is often used to enhance the permeability of natural fracture networks in deep low-permeability reservoirs. The downside of hydraulic stimulation is that it may trigger or induce felt seismicity on pre-existing fractures or faults. Key to a successful development of enhanced geothermal systems is stimulation of rocks in order to sufficiently enhance flow rates, whilst keeping magnitudes of induced earthquakes at acceptable levels - so-called 'soft' hydraulic stimulation.

The hydro-mechanical model in TOUGH-Flac^{3d} was used to simulate the effect of hydraulic stimulation on the potential of fault reactivation and associated seismicity. Using the TOUGH-Flac^{3d} simulator, we take into account the full coupling between the hydraulic and mechanical processes affecting the evolution of permeability and flow through the reservoir rocks and the mechanical response of the fault system. We model injection into a single well, at close distance to a steeply dipping fault, which is bounded by a fault damage zone and embedded in a low-permeability rock matrix. We analyze the impact of the transmissivity of the fault core on fault stresses and loading rates, both during the injection period and after shut-in of the injection well. We discuss the effect of fault properties on the evolution of induced seismicity through the rate-and-state model, both during and after hydraulic stimulation. This way, we build a further understanding of physical mechanisms which drive fault reactivation and induced seismicity, which may help in the future design of soft hydraulic stimulation strategies.

1. INTRODUCTION

For a successful development of enhanced geothermal systems (EGS) in deep, low-permeability rocks, hydraulic stimulation of the pre-existing natural fracture networks is needed in order to enhance injectivity and flow rates. However, hydraulic stimulations may also trigger or induce felt seismicity. Hence it is important to optimize stimulation in such a way as to minimize magnitudes of induced earthquakes. Recently in the literature, a number of soft stimulation strategies have been proposed as an option to mitigate seismicity during stimulation operations. Concepts for soft hydraulic stimulation have been described in Zang et al (2013), Zimmermann et al (2015), Huenges et al (2017 and this issue) and Hofmann et al (2018, 2019, this issue). These soft hydraulic stimulation techniques may encompass techniques such as cyclic and multistage stimulation, and other measures such as the application of a gradual shut-in of the injection well to avoid a fast release of poroelastic stresses and associated seismicity after shut-in (Segall et al (2015)), well bleed-off and flowback. For the design of soft hydraulic stimulations, we need a further understanding of the processes that drive fault reactivation and induced seismicity during (and after) hydraulic stimulation.

Here we use a 3D coupled hydro-mechanical numerical model in combination with the rate-and-state seismicity theory of Dieterich (1994) to investigate the effect of hydraulic stimulation for EGS on fault reactivation and associated seismicity. We use the software code of TOUGH-Flac^{3d} (Taron and Elsworth 2010, Gan and Elsworth 2014) for modelling the fully coupled hydro-mechanical processes, and related pressure and stress changes in the rocks and at the faults. We model fluid injection into a single well, at close distance to a single fault, bounded by a fault damage zone and embedded in a low-permeability rock matrix. In a recent paper by Chang and Yoon (2018) it was shown that the presence of low-permeability faults nearby injection wells can affect pressure and poroelastic changes, and thereby influence fault reactivation and seismicity. In this study, we further investigate the effect of fault zone hydrological properties on the evolution of seismicity in space and time.

2. MODELLING APPROACH

In the TOUGH-Flac^{3d} simulation the full coupling between the hydraulic and mechanical processes affecting flow through the reservoir and the mechanical response of the fault system are accounted for. We model injection into a single well in the hanging wall block close to a steep fault. The fault core is bounded by a 50m wide high-permeability fault damage zone and embedded in a low-permeability rock matrix. We analyze the impact of the transmissivity of the fault core on fault stresses, loading rates and related seismicity, both during the injection period and after shut-in of the injection well. At this stage we are not aiming at modelling a specific EGS field case, though chosen conditions can be considered as being representative of some of the geological conditions encountered at a number of EGS sites, as geothermal systems frequently target the high-permeability damage zones of fault structures in the crystalline basement or low-permeability clastic reservoirs (e.g. in some of the geothermal sites in the Lower Rhine Graben (Vidal and Genter 2018) or the Pohang EGS site where stimulation took place in an injection well within or very close to the damage zone of a large critically stressed fault (Hofmann et al., 2018 and 2019, Kim et al., 2017, Grigoli et al., 2017, Ge et al., 2019).

The fault is modelled at a depth between 3700m and 4700m below surface level, with dimensions of 1 km (height) by 3 km (width) at a dip of 70º. The finite-difference model grid is aligned with the strike of the fault (see Fig.1). Model dimensions are 3 km × 3 km × 2 km. All vertical model boundaries are fixed horizontally and the lower horizontal boundary is fixed in a vertical direction. A vertical stress is imposed on the upper boundary of the model and represents the weight of the overburden. For fluid injection we assume that a direct hydraulic connection, representative of e.g. the presence of a hydraulic fracture or pre-existing natural fracture, exists between the damage zone and the injection well. Fluid is injected directly into the damage zone at a distance of approximately

50 m from the fault. Fluids are injected at a constant injection rate of 10 L/s during just over 55 hours, and the total volume injected before shut-in of the well is 2000 m^3. The total period modelled is 28 days.

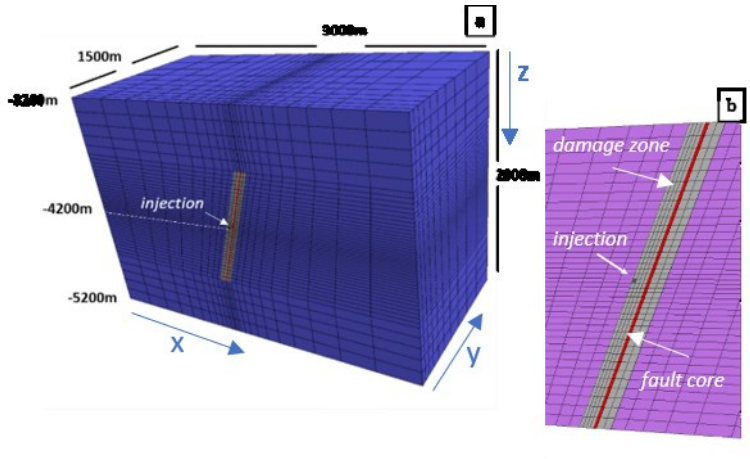

Figure 1: a) Geometry of the fault (red), damage zone (grey) and matrix rocks (blue); b) detail of the fault zone and location of injection. Half of the model shown (model has been cut by a vertical plane oriented perpendicular to the y-axis, through the injection point).

We assume an initial strike slip tectonic regime, with SHmax > Sv > shmin and maximum horizontal stress SHmax oriented at an oblique angle (approximately 70°) to the strike of the fault (right-lateral strike slip conditions). We assume hydrostatic pressure gradients, a total maximum horizontal stress gradient of 31 MPa/km, a total minimum horizontal stress gradient of 19 MPa/km and a total vertical stress gradient of 26 MPa/km.

We monitor the spatial and temporal evolution of pore pressures and stresses on the fault. We calculate Coulomb stress changes from changes in pore pressures and normal and shear stresses on the fault plane. Coulomb stresses changes ($\Delta\tau_{cs}$) result from the increase of pore pressures, due to diffusion into the fault (which we here refer to as the 'direct pore pressure effect') and poroelastic stress changes, caused by the deformation of the rocks. Coulomb stress changes can be written, in terms of total stress:

$$\Delta\tau_{cs} = (\Delta\tau_s - \mu\Delta\sigma_n + \mu\Delta P) \tag{1}$$

Where Δ denotes a change, τ_s is shear stress, σ_n is total normal stress on the fault, μ is friction coefficient of the fault and P is pore pressure in the fault. Positive Coulomb stress changes are indicative of a destabilizing stress path on the fault, whereas fault segments with negative Coulomb stress changes are stabilizing. If we look at the latter equation, we see the first two components on the right hand side denote the contribution of poroelastic stress changes on the fault, whereas the last component gives the contribution of the 'direct' pore pressure effect.

We now can derive Coulomb stressing rates from the evolution of Coulomb stress changes over time, which we then use to obtain relative seismicity rates, based on the theory of rate-and-state seismicity (Dieterich 1994, Segall et al 2015):

$$\frac{dR}{dt} = \frac{R}{t_a}\left(\frac{\dot{\tau_{cs}}}{\dot{\tau_0}} - R\right) \tag{2}$$

Here R is relative seismicity rate (which is the seismicity rate divided by background seismicity rate) and $\dot{\tau}_0$ is tectonic stressing rate. The t_a in the equation is a decay parameter, defining how long it takes for seismicity to decay to its background seismicity rate, following a large stress perturbation. The magnitude of t_a depends on background stressing rate, fault parameter A which quantifies the direct effect of rate and state friction behavior of the fault and normal effective stress σ'_n:

$$t_a = \frac{A\dot{\tau}_0}{\sigma'_n} \tag{3}$$

Here, we assume A = 0.001, and $\dot{\tau}_0$ of 0.0002 MPa/yr, which results in a time decay $t_a \approx 100$ years. This time decay factor t_a will affect the delay between stress perturbations and the seismic response of the fault. For a very short t_a relative to the duration of the perturbation, the predicted seismicity rates will follow the trend of Coulomb stressing rates; for very large t_a (relative to the perturbation), seismicity rates will follow the pattern of the Coulomb stress changes (Ader et al., 2014).

To analyze the effect of fault transmissibility on fault Coulomb stressing, we define three scenarios for the transmissibility of the fault core. In all scenarios, fault, damage zone and rock matrix are characterized by uniform permeability and homogeneous elastic properties. Permeability and elastic properties for the fault, damage zone and matrix are summarized in Table 1. First we look at the response of two end-members, i.e. a sealing fault with a very low permeability and an open fault with high permeability. In case of the open fault no distinction is made between the permeability and porosity of the fault and the damage zone. In addition, we define a base-case scenario in which we assign properties to the fault, damage zone and matrix which are representative for a fault zone in granitic rocks.

Table 1: Permeability and elastic properties of the model

Parameters	Matrix	Damage zone	Sealing fault	Open fault	Partially sealing fault
(Across fault) permeability	isotropic	isotropic	0.5e-20m2	3.0e-15m2	2.0e-19m2
Porosity	0.01	0.05	0.001	0.05	0.001
Bulk modulus	33GPa	33GPa	33GPa	33GPa	33GPa
Poisson's ratio	0.25	0.25	0.25	0.25	0.25

3. MODELLING RESULTS

3.1 Two End-members: Open and Sealing Fault

In Figure 2 we present the spatial distribution of changes in pore pressures, total normal stresses and shear stresses and resulting Coulomb stress changes at the end of the injection period after around 55 hours of injection into the well, for the two end-member scenarios, i.e. an open (Figure 2a) and a sealing (Figure 2b) fault structure. We observe significant differences in the spatial pattern of pressures and stresses, caused by the difference in fault transmissivity. In both cases, we see a distribution of elevated pore pressures and total normal stresses in the fault (core), which is concentric around the fault location nearest to the injection well. At the end of injection, pore pressures at the fault location nearest to the injection well are higher for the open fault than for the sealing fault. The evolution of shear stresses in both cases is quite different. For the high fault permeability, pore pressure changes occur in both the hanging- and footwall block, and cause rock volumes on both sides of the fault to expand. Hence, only small differential movements along the fault occur, resulting in relatively small shear stresses. In case of a low permeability fault core, poroelastic volumetric expansion of the rocks occurs solely in the hanging wall block of the fault and causes additional shear stresses on the upper segment of the fault above and to the NE of the injection well, adding to the shear stresses already present from the tectonic loading. Increments in shear stresses on the lower and SW fault segment however counteract the initial tectonic shear stresses and lead to a stabilizing effect on this part of the fault. Here, the contribution of shear stresses results in a stabilization of the lower SE section of the fault, which is not observed in case of the open fault.

We disentangle the contribution of the three components of total normal stress, shear stress and pore pressure (see also equation 1) to fault loading in Figure 3, which shows the evolution of the three components in time. We monitor the response at the fault location nearest to the injection point. For the open fault, during the injection phase (before shut-in of the well) pore pressure effects are dominant, and Coulomb stress changes are highest, as pore pressures can rapidly diffuse into the fault (Figure 3a). For the sealing fault, direct pore pressure effects are smaller during the injection phase, as pore pressures diffusion into the low permeability fault core is lower (Figure 3b). On the other hand, the contribution of shear stresses during the injection phase to the Coulomb stress change is much larger in case of the sealing fault. Total normal stress changes are of the same order of magnitude, though slightly higher in case of the open fault. We can observe from Figure 3 that after shut-in, for the open fault changes in Coulomb stresses in the area around the injection well are negative. Here shut-in of the well thus leads to a rapid decline of pore pressures and associated stabilization of the fault in the near-well area. In case of the sealing fault, pore pressures remain relatively high after shut-in, as the decrease in pore pressures is much more gradual due to low fault permeability. For the sealing fault, the response after shut-in is dominated by the immediate release of poroelastic stresses. Although shear stresses and pore pressures do diminish after shut-in, the clamping forces of the normal stresses reduce significantly. The latter being the largest and immediate effect, a rapid but temporary increase of Coulomb stresses in the near-well fault segment is observed at shut-in of the well. A similar effect has been described by Segall and Lu (2015) for a homogeneous rock mass.

3.2 Coulomb Stressing Rates and Seismicity Rates

We can now derive Coulomb stressing rates and associated seismicity rates from the evolution of Coulomb stress changes (figure 4). We monitor stressing rates and seismicity rates for three different locations, i.e. at the location of largest Coulomb stress changes (blue), at the location nearest to the injection well (red) and at the location of largest seismicity rates (green). For the open fault (Figure 4a, c and e), maximum Coulomb stress changes, maximum stressing rates and maximum seismicity rates all occur at the fault location close to the injection point, so the two curves overlap. For the sealing fault, maximum Coulomb stresses and maximum seismicity rates occur at different fault locations. For the sealing fault we observe a sharp peak in both stressing rates and seismicity rate after shut-in of the injection well, which is related to the sudden increase in Coulomb stresses after shut-in shown in Figure 3b (see green and red curve, figure 4d and f). For the location with maximum Coulomb stress changes, seismicity rate reaches a peak value some time after the onset of the stimulation (see blue curve, figure 4f).

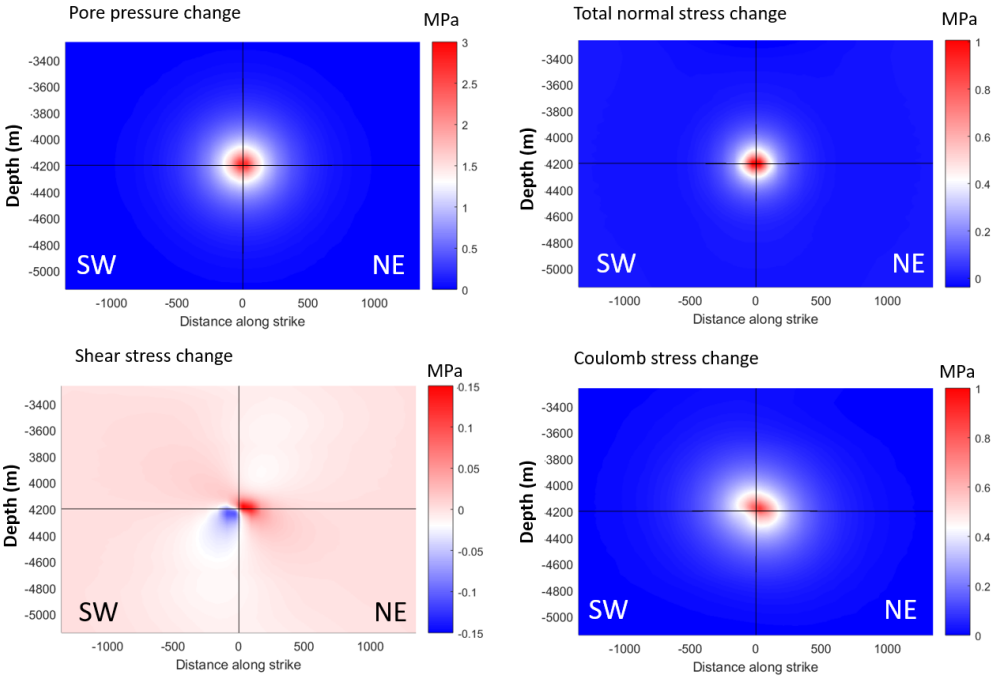

Figure 2a: Spatial distribution of changes in pore pressure, total normal stress, shear stress and Coulomb stress on the fault with high permeability ('open fault'). Horizontal continuous black line indicates depth (z) of injection. Vertical continuous black line indicates horizontal position of injection well (in y-direction parallel to the strike of the fault). Injection takes place at a distance of approximately 50m from the fault (in x--direction, perpendicular to fault plane).

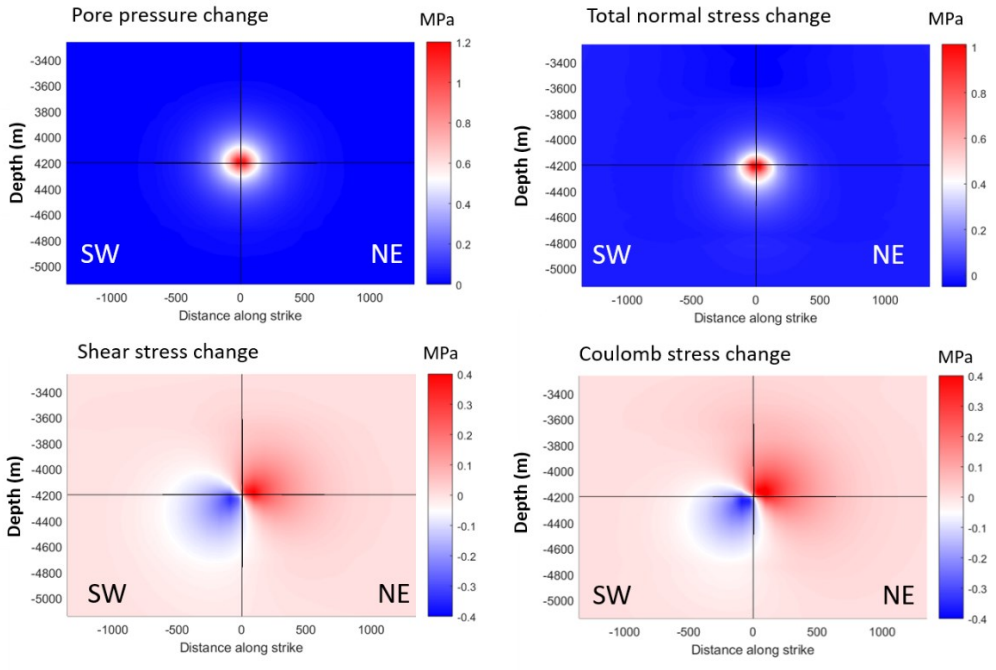

Figure 2b: Spatial distribution of changes in pore pressure, total normal stress, shear stress and Coulomb stress on the fault with low permeability ('sealing fault'). Horizontal continuous black line indicates depth (z) of injection. Vertical continuous black line indicates horizontal position of injection well (in y-direction parallel to the strike of the fault). Injection takes place at a distance of approximately 50m from the fault (in x--direction, perpendicular to fault plane). Mark: scale of legend is different from Figure 2a.

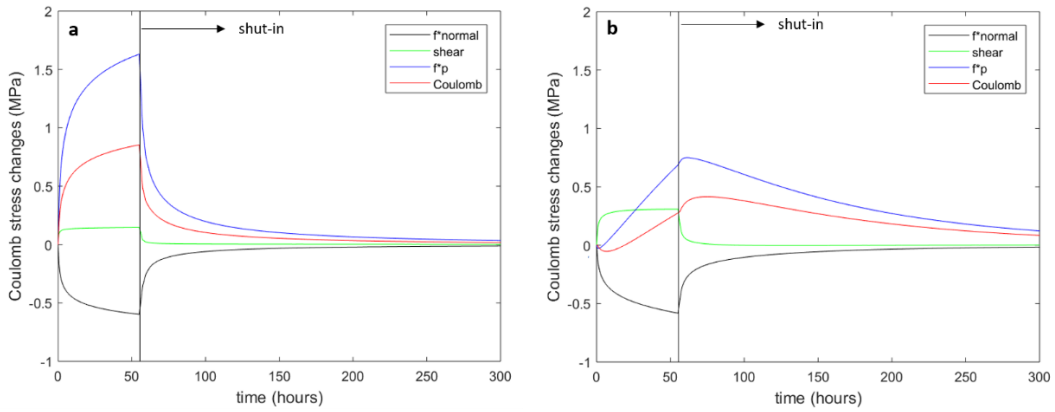

Figure 3: Contribution of changes in pore pressure, total normal stress, shear stress to Coulomb stress changes on the fault, for the fault with a) high permeability ('open fault') and b) low permeability ('sealing fault'), monitored at the fault location nearest to the injection location.

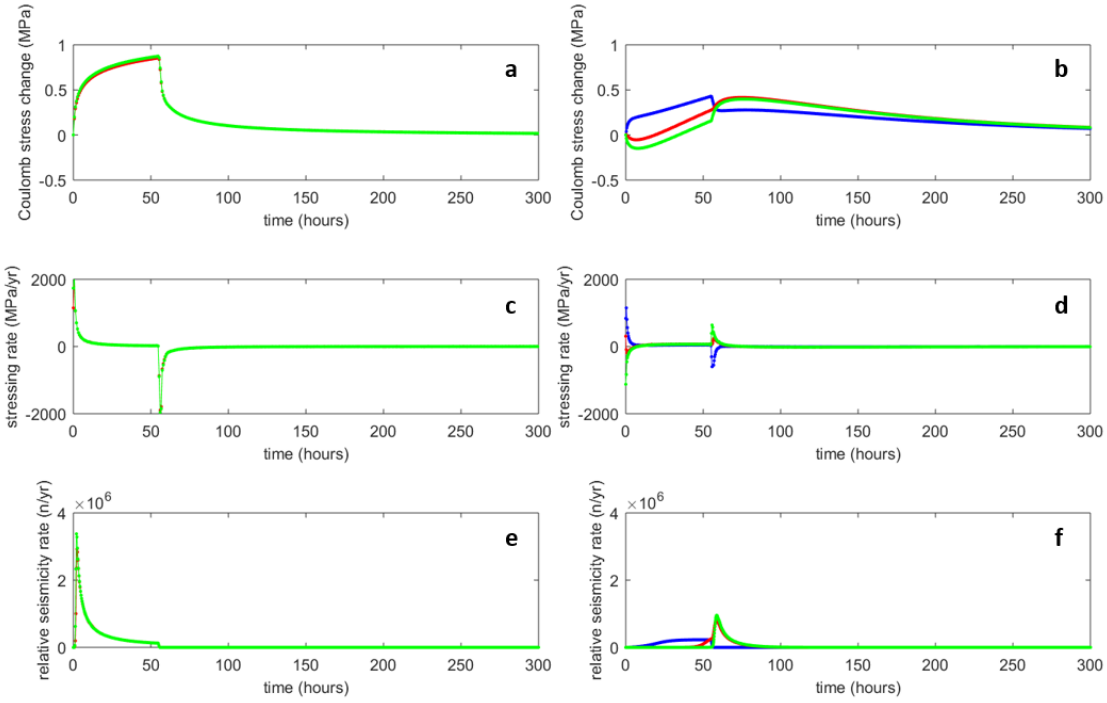

Figure 4: Coulomb stress change (a, b), Coulomb stressing rates (c, d) and seismicity rates (e, f) for the (a, c, e) open fault and (b, d, f) sealing fault. Green line: changes at location of highest coulomb stress change; blue line: changes at location of highest seismicity rates, red line: changes at location nearest to injection well.

3.3 Seismic Response of Partially Sealing Fault

In addition to the two end-members defined before, we define a scenario for a partially sealing fault, with permeabilities of core, damage zone and matrix rocks characteristic for a fault zone in granitic rocks. Parameters are summarized in Table 1. The response of the partially sealing fault in terms of Coulomb stress changes, stressing and seismicity rates is shown in Figure 5. The partially sealing fault shows an intermediate response between the response of the open and sealing fault. Figure 5a-b show the contribution of pore pressures, total normal and shear stress to Coulomb stress changes for the location with maximum Coulomb stress change and maximum seismicity rate. The contribution of pore pressures is relatively high (Figure 5a-b) and can be explained by the fact that pore pressure build up in the injection well and hanging wall fault block is high, and steep gradients in pore pressure develop over the fault core. In addition, the pressure gradient over the fault core, and associated differential expansion of the rock mass on both sides of the fault cause a significant contribution of poroelastic effects. Due to the relatively large contribution of shear to loading during the injection phase, the fault section below and to the SW of the injection stabilizes during the injection phase, but as pore pressures are higher, this stabilizing area is much smaller than for the sealing fault (Figure 5e).

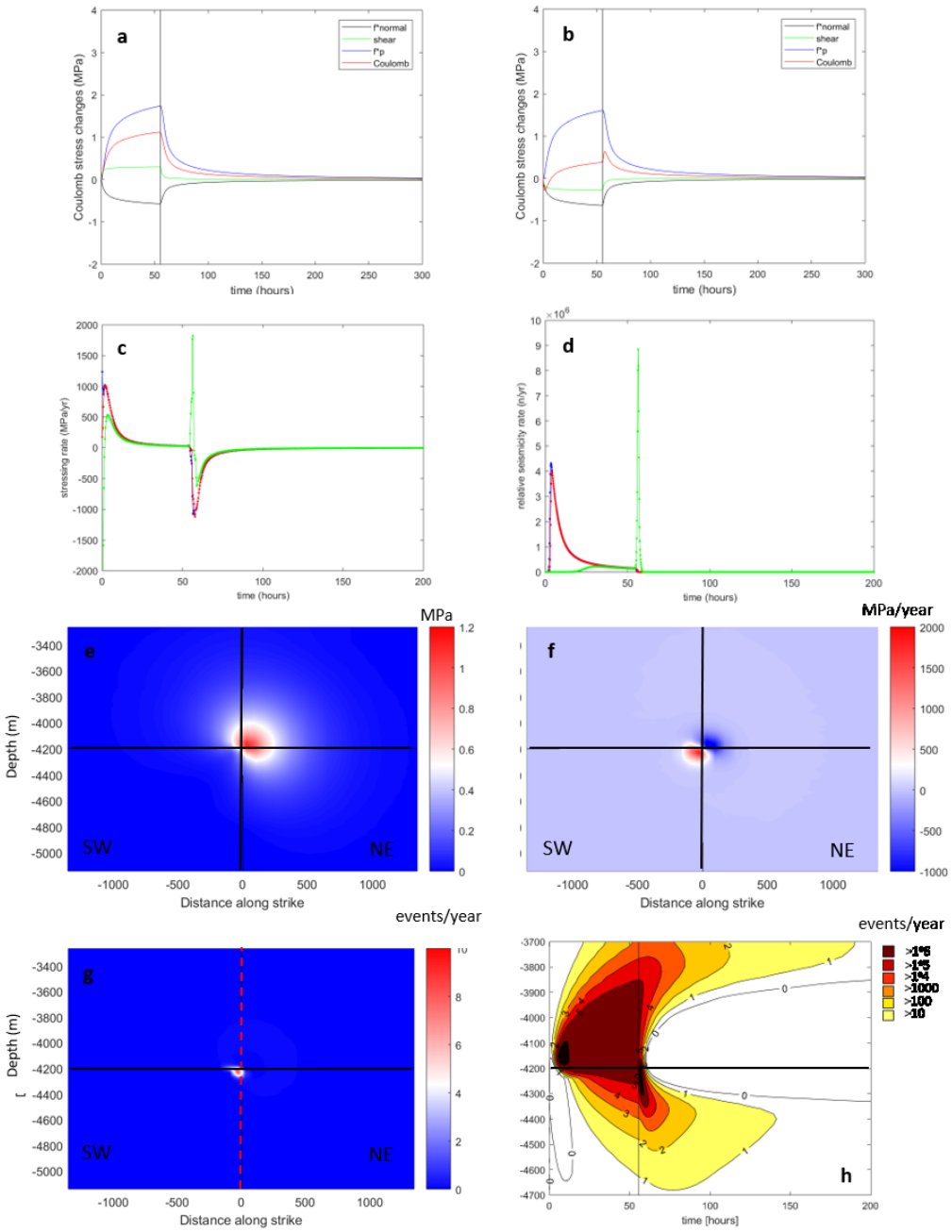

Figure 5: a) Temporal evolution of changes in pore pressure (blue), total normal stress (black), shear stress (green) and Coulomb stress changes (red) on the fault, for a partially sealing fault, monitored at the fault location with maximum Coulomb stress change, b) temporal evolution of changes in pore pressure (blue), total normal stress (black), shear stress (green) and Coulomb stress changes (red) on the fault, for a partially sealing fault, monitored at the fault location with maximum seismicity rate, c) temporal evolution of Coulomb stressing rates at fault location with maximum Coulomb stress change (red), nearest to the injection well (blue) and highest seismicity rate (green), d) temporal evolution of seismicity rates at fault location with maximum Coulomb stress change (red), nearest to the injection well (blue) and highest seismicity rate (green), e) spatial distribution of Coulomb stress changes at end of injection period just before shut-in (~55hours), f) spatial distribution of Coulomb stressing rates just after shut-in (~56 hours) g) spatial distribution of seismicity rates just after shut-in (56 hours) and h) temporal and spatial distribution of seismicity rates along a 2D line within the fault core, oriented in dip-direction and intersecting the location of peak seismicity rates (i.e. along red dashed line presented in Fig.5b) . Dark colors denote high seismicity rates (log-scale).

For this area, rapid poroelastic unloading after shut-in leads to a rapid destabilization, which results locally in high Coulomb stressing and seismicity rates (see Figure 5 f-g). Seismicity rates just after the start of injection are similar to the open fault, but higher than for the sealing fault, whereas seismicity rates after shut-in are higher than seismicity rates encountered for both the open and sealing fault. Figure 5h shows a peak in seismicity in the upper fault segment, just after the start of injection, and the sharp peak in seismicity just after shut-in of the injection well in the lower fault segment, followed by a stabilization of the area around the injection well. It also shows seismicity spreading up and downwards in time, which may be due to the effect of ongoing pore pressure diffusion, after shut-in of the well, and the time delay in seismic response of the fault (t_a).

4. DISCUSSION AND CONCLUSIONS

The hydro-mechanically coupled model in Tough-Flac^{3D} enables the evaluation of the relative contribution of direct pressure and poroelastic effects to fault stressing. Our models show that fault transmissivity determines the 3D spatio-temporal pattern of Coulomb stresses and stressing rates, and the associated seismicity near an injection well. For the temporal evolution of seismicity, our modelling results show that the direct pore pressure effect dominates the seismic response of the fault in case of an open fault, causing highest stressing and seismicity rates just after the start of injection and a rapid decline of seismicity spreading from the injection well after shut-in of the well. For the sealing fault, poroelastic effects are dominant, whereas the partially sealing fault shows a balance between poroelastic and direct pore pressure effects. Both the sealing and partially sealing fault show a peak in seismicity rate immediately after shut-in, caused by a rapid release of poroelastic stresses. Insights into the contribution of direct pore pressures and poroelastic effects to fault loading will provide direct implications in the design of soft stimulation measures, such as e.g. reduction of post shut-in seismicity rates by a tapering of the shut-in of the injection well (Segall and Lu, 2015). In addition to driving the temporal distribution, we also see that the permeability of the fault strongly influences the spatial pattern of seismicity. It is noted here that next to fault transmissibility, other subsurface properties such as damage zone and matrix flow properties, mechanical properties such as stiffness of the fault core, damage zone and matrix, as well as fault geometry and tectonic setting, and operational parameters like location and distance of the injection well to the fault will have an effect on the relative contribution of poroelastic and direct pore pressure effects, and hence also on the spatial and temporal distribution of the seismicity. Moreover, the timing and shape of the seismicity peaks will be determined by the rate-and-state fault parameters (e.g. t_a). In practice many of these parameters will be uncertain, and difficult to determine prior to the hydraulic stimulation operations. However, the results of this study indicate that modelling combined with a close monitoring of the spatial and temporal distribution of seismicity may help to further constrain some of the unknown subsurface parameters, such as e.g. fault transmissivity.

ACKNOWLEDGEMENTS

The project leading to part of the results in this article received funding from the European Union's Horizon 2020 research and innovation programme under grant agreement No 691728.

REFERENCES

Ader, Th., Lapusta, N., Avouac, J.P. and Ampuero, J.P.: Response of rate-and-state seismogenic faults to harmonic shear-stress perturbations, *Geophys. J. Int.* (2014), 198, 385-413.

Chang, K.W., Yoon H.: 3-D Modeling of Induced Seismicity along Multiple Faults: Magnitude, Rate and Location in a Poroelasticity System, *J. Geophys. Res. Solid Earth* (2018), 123.

Dieterich, J.: A constitutive law for rate of earthquake production and its application to earthquake clustering. *J. of Geophys. Research* (1994), 99 B2, 2601-2618.

Gan, Q. and Elsworth, D. Thermal drawdown and late-stage seismic-slip fault reactivation in enhanced geothermal reservoirs. *J. Geophys. Res. Solid Earth* (2014), 119, 8936-8949.

Grigoli, F., Cesca, S., Rinaldi, A.P., Manconi, A.,Lopez-Comino, J.A., Clinton, J.F., Westaway, R., Cauzzi, C., Dahm, T. and Wiemer, S.: The November 2017 Mw 5.5 Pohang earthquake: A possible case of induced seismicity in South Korea. *Science* 10.1126/science.aat2010 (2018).

Huenges, E., Zang, A., Kim, K.Y.: Soft stimulation and induced seismicity, Schatzalp workshop on Induced seismicity, Davos, Switzerland, 14-17, (2017).

Hofmann, H., Zimmermann, G., Zang, A., Min, K.B.: Cyclic Soft stimulation (CCS0: A new fluid injection protocol and traffic light system to mitigate seismic risks of hydraulic stimulation treatments, *Geotherm Energy* (2018), 6:27.

Hofmann, H., et al.: First field application of cyclic soft stimulation at the Pohang Enhanced Geothermal system site in Korea, *Geophys. Intern.* 217, pp 926-949 (2019).

Kim, K.H., Ree, J.H., Kim, J.H., Kim, S., Kang, S.Y., Seo, W.: Assessing whether the 2017 Mw 5.4 Pohang earthquake in South Korea was an induced event. et al 2018. *Science* 10.1126/science.aat6081 (2018).

Ge, S., Giardini, D., Ellsworth, W., Shimamoto, T., Townend, J., 2019. Overseas research Advisory Committee report on the Pohang Earthquake.

Segall, P., Lu, S.: Injection-induced seismicity: Poroelastic and earthquake nucleation effects. *J. Geophys. Res. Solid Earth* (2015), 120, 5082-5103.

Taron, J. and Elsworth, D.: Coupled mechanical and chemical processes in engineered geothermal reservoirs with dynamic permeability, International journal of rock Mechanics and Mining Sciences (2010, 47, 1339-1348.

Vidal J. and Genter A.: Overview of naturally permeable fractured reservoirs in the central and southern Upper rhine Graben: Insights from geothermal wells, *Geothermics* (2018), 74, 57-73.

Zang, A., Yoon, J.S., Stephansson, O. and Heidbach, O.: fatigue hydraulic fracturing by cyclic reservoir treatment enhances permeability and reduces induced seismicity, *Geophys. J. Int.* (2013), 195(2), 1282-1287.

Zimmermann, G., Hofmann, H., Babdagli, T., Yoon, S.J., Zang, A., Deon, F., Urpi, L., Blocher, G., Hassanzadegan, A., and Huenges, E.: Multi-fracturing and cyclic hydraulic stimulation scenarios to develop enhanced geothermal systems – feasibility and mitigation strategies to reduce seismic risk, *Proceedings of the World Geothermal Congress 2015*, Melbourne, Australia, 19-25 April (2015), paper #31009.